Materials Today Chemistry 22 (2021) 100596

Contents lists available at ScienceDirect

Materials Today Chemistry

journal homepage: www.journals.elsevier.com/materials-today-chemistry/

Dual removal and selective recovery of phosphate and an organophosphorus pesticide from water by a Zr-based metal-organic framework

L. González [a], F.J. Carmona [a, *], N.M. Padial [b], J.A.R. Navarro [a], E. Barea [a], C.R. Maldonado [a, **]

[a] Departamento de Química Inorgánica, Universidad de Granada, Av. Fuentenueva S/N, Granada, 18071, Spain
[b] Functional Inorganic Materials Team, Instituto de Ciencia Molecular (ICMol), Universitat de València, 46980 València, Spain

ARTICLE INFO

Article history:
Received 4 August 2021
Received in revised form
10 September 2021
Accepted 13 September 2021
Available online xxx

Keywords:
Eutrophication
Phosphorous circular economy
Organophosphates
Water decontamination

ABSTRACT

Zr-based metal-organic framework $[Zr_6(\mu_3\text{-}O)_4(\mu_3\text{-}OH)_4(OH)_4(H_2O)_4$(1,3,6,8-tetrakis(*p*-benzoate)pyrene$)_2]$ (**NU-1000**) has been successfully used to remove phosphate and fenamiphos (an organophosphorus pesticide) from water solutions. In order to approach practical conditions, these studies have been performed under dynamic conditions and in the presence of relevant interferences, such as hydrogen carbonate. The results show that **NU-1000** is able to adsorb 0.19 mol/mol of phosphate, reaching a plateau after 20 min, while 0.89 mol/mol fenamiphos is captured after 120 min. Afterward, a three-step strategy has been designed, allowing quantitative recovery of both phosphate anions and fenamiphos, separately, and ulterior adsorbent regeneration. Noteworthy, after this treatment, **NU-1000** maintains a good performance toward the dual removal and selective desorption of phosphate and fenamiphos for at least two additional cycles.

1. Introduction

One of the greatest challenges of the 21st century is to increase the production of crops to satisfy the high demand of food of the ever-growing global population (from the current 7.6 billion to the 10 billion expected by 2050) [1]. This challenge involves a significant increment of global production and the use of agrochemicals, including fertilizers and pesticides, in order to maximize crop yields. However, this goal also poses real threats to human health, aquatic ecosystems, and the environment at large. One of the most common classes of pesticides, namely organophosphates, is highly toxic to humans and ecosystems due to their acetylcholinesterase inhibition activity [2]. As a result, negative effects on the organism ranging from paralysis to seizures and eventually death may take place. Another problem associated with agricultural sustainability is the intensive use of phosphate fertilizers, which are obtained from non-renewable phosphate rock sources. While 90% of mined phosphate rock is used for food production, only one-fifth of it reaches the global food chain, with the major share being leaked to soil/aquatic media leading to severe environmental problems (eutrophication) [3]. For this reason, the design of new strategies aimed at contributing to the P circular economy is of paramount importance.

Existing technologies for pollutant remediation include precipitation, membrane technology, coagulation/flocculation, biological processes, advanced oxidation, and adsorption. However, these conventional decontamination methods suffer from high operating costs, generation of secondary pollutants, and partial removal of contaminants. Thus, there is a high interest in developing non-toxic and efficient materials for pesticide decontamination and phosphate recovery. These materials should be easily regenerated in order to be reused in successive adsorption-desorption cycles.

In this context, metal-organic frameworks (MOFs), which are crystalline porous materials based on metal clusters connected by organic spacers, are being thoroughly studied for environmental pollutants detoxification [4] [–] [7]. Among them, non-toxic zirconium MOFs, based on $Zr_6O_4(OH)_4$ secondary building units, have shown to be chemically stable [8] and to adsorb phosphate ions [9–11]or pesticides efficiently [12–15]. However, these studies are focused on the removal of a single pollutant through batch processes, far from the real applications.

* Corresponding author.
** Corresponding author.
E-mail addresses: fjcarmona@ugr.es (F.J. Carmona), crmaldonado@ugr.es (C.R. Maldonado).

https://doi.org/10.1016/j.mtchem.2021.100596

In this work, we have selected **NU-1000** ($[Zr_6(\mu_3\text{-}O)_4(\mu_3\text{-}OH)_4(OH)_4(H_2O)_4(TBAPy)_2]$, TBAPy = 1,3,6,8-tetrakis(*p*-benzoate) pyrene, a robust and low connectivity material with hierarchical micro/mesoporous structure, for the simultaneous capture and selective recovery of phosphate fertilizer and fenamiphos ((*RS*)-*N*-[ethoxy-(3-methyl-4-methylsulfanylphenoxy)phosphoryl] propan-2-amine)) pesticide under dynamic conditions, approaching wastewater treatment close to realistic situations (Scheme 1).

2. Material and methods

2.1. General methods

All chemicals were commercially available and used without further purification. Powder X-Ray diffraction (PXRD) data were obtained on a X'Pert PRO diffractometer (PANalytical) with the following instrumental parameters: Cu Kα radiation ($\lambda = 1.5405$ Å), current = 40 mA, tension = 45 kV, measurement range $2\theta = 3º\text{-}50º$, time per step = 4 s, and step size = 0.04º 2θ. For the adsorption recyclability assays, XRPD data were collected on a Bruker D2 PHASER Bruker diffractometer: Cu Kα radiation ($\lambda = 1.5418$ Å), measurement range $2\theta = 5º\text{-}45º$, time per step = 0.5 and step size = 0.02º. Before each measurement, the samples were manually grounded in an agate mortar and then deposited in the hollow of a zero-background silicon sample holder. Infrared spectra were collected in a Fourier transform infrared spectrophotometer Bruker Tensor 27 (32 scans, resolution = 2 cm^{-1}). Thermogravimetric analyses were performed using a Mettler Toledo TGA/DSC STAR system under airflow (20 mL/min) running from room temperature to 900 °C with a heating rate of 2 °C/min (CIC, University of Granada). Elemental (C, H, N) analyses were obtained with a Flash EA1112 CHNS-O instrument (CIC, University of Granada). Nitrogen adsorption isotherms were measured at 77 K on Micromeritics *Tristar 3000* and *3flex* volumetric instruments. The samples were heated 12 h at 393 K and outgassed to 10^{-1} Pa before the adsorption measurements. UV-vis spectra were collected on a Shimadzu UV spectrophotometer. Inductively coupled plasma mass spectrometry analysis (ICP-MS) was carried out with a NexION 300D instrument (CIC, University of Granada).

2.2. Batch adsorption experiments

2.2.1. Adsorption isotherms of fenamiphos and phosphate

The adsorption capacity of **NU-1000** for phosphate and fenamiphos was first assessed separately. In particular, aqueous solutions of phosphate or fenamiphos (0.05 mM) were mixed with different aqueous suspensions of **NU-1000** (10.9 mg/L − 108.8 mg/L). In addition, aqueous solutions of phosphate or fenamiphos (0.05 mM) without MOF, as well as suspensions of **NU-1000** (10.9 mg/L − 108.8 mg/L) were also prepared as controls. All samples were shaken at 25 °C for 24 h, and the supernatant was collected by centrifugation (9168 g/15 min). The concentration of fenamiphos in the supernatants was determined spectrophotometrically ($\lambda_{max} = 248$ nm), while the concentration of phosphate was analyzed by means of the molybdenum blue method [17]. All the experiments were performed in triplicate.

The adsorption capacity of **NU-1000** was calculated as follows (Equation (1)):

$$q = \frac{c_o - c_e}{c_{MOF}} \quad (1)$$

q = adsorption capacity (mol/mol)

c_o = initial concentration of fenamiphos or phosphate (mM)

c_e = concentration of fenamiphos or phoshate (mM) after 24 h of adsorption

c_{MOF} = concentration of NU-1000 (mM) in the aqueous suspension

Finally, the experimental data were fitted to adsorption Langmuir equation (Equation (2)):

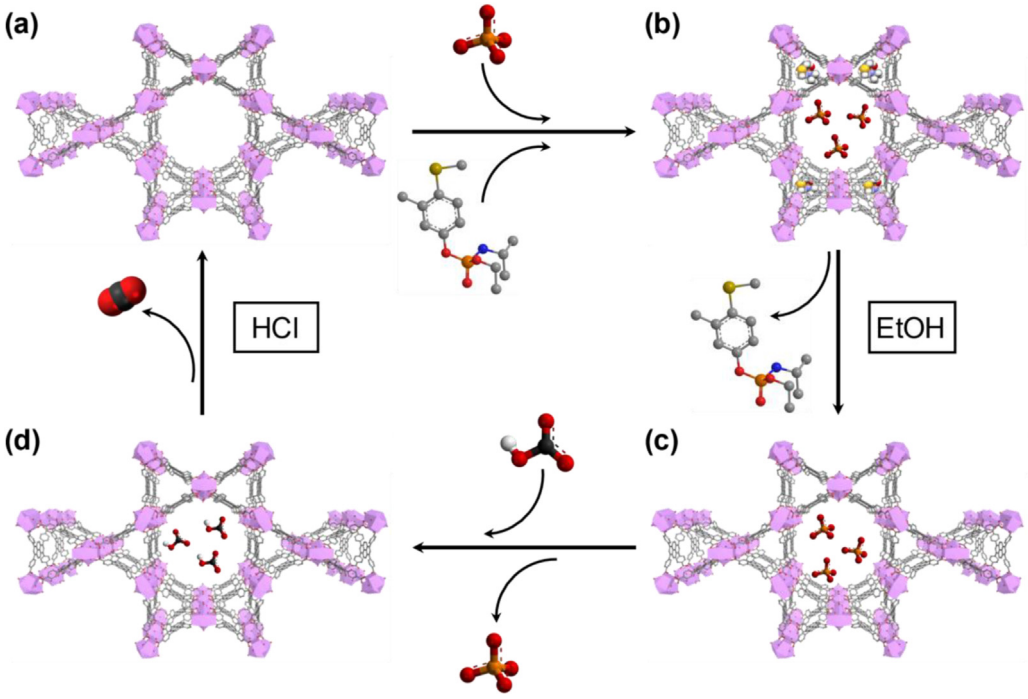

Scheme 1. Strategy for the reversible and selective phosphate and fenamiphos capture and recovery by **NU-1000**. (a) Simultaneous adsorption process. (b) Desorption of fenamiphos with ethanol. (c) Ion exchange of phosphate with hydrogen carbonate. (d) Regeneration of **NU-1000** by treatment with hydrochloric acid.

$$q_e = \frac{q_{max} \cdot k \cdot c_e}{1 + k \cdot c_e} \quad (2)$$

q_e = adsorption capacity (mol/mol) after 24 h of adsorption
q_{max} = maximum adsorption capacity (mol/mol)
k = Langmuir constant of adsorption (L/mol)

2.2.2. Adsorption kinetics of fenamiphos and phosphate

Aqueous suspensions (1 mL) containing **NU-1000** (108.8 mg/L) and fenamiphos or phosphate (0.05 mM) were shaken at 25 °C for 30, 60, 210, 330 and 1440 min. At each time, the supernatant was collected by centrifugation (9168 *g*/15 min). As previously mentioned, the concentration of fenamiphos was determined spectrophotometrically (λ_{max} = 248 nm), while the concentration of phosphate was determined by means of the molybdenum blue method [17]. All the experiments were performed in triplicate.

All experimental data were fitted to a *pseudo*-second-order model, according to Equation (3):

$$q_t = \frac{q_e^2 \cdot k_t \cdot t}{1 + q_e \cdot k_t \cdot t} \quad (3)$$

t = time of adsorption (min)
q_t = adsorption capacity (mol/mol) at time t
q_e = equilibrium adsorption capacity (mol/mol)
k_t = adsorption rate constant (mol/mol/min)

2.2.3. Simultaneous adsorption of fenamiphos and phosphate

Aqueous suspensions (1 mL) containing equimolar amounts of **NU-1000** (108.8 mg/L), phosphate, and fenamiphos (0.05 mM) were shaken at 25 °C for 30, 60, 210, 330, and 1440 min. At each time, the supernatant was collected by centrifugation (9168 *g*/15 min). As mentioned before, the concentration of fenamiphos was determined spectrophotometrically (λ_{max} = 248 nm), while the concentration of phosphate was analyzed by means of the molybdenum blue method [17]. All the experiments were performed in triplicate.

2.2.4. Adsorption experiments in the presence of relevant interferences

Adsorption experiments in the presence of potential interferences typically found in water, namely sodium chloride, sodium sulfate, sodium nitrate, and sodium hydrogen carbonate, were performed in order to evaluate the selectivity of NU-1000 toward phosphate and fenamiphos.

In a typical experimental, aqueous suspension (1 mL) containing one of the previously mentioned interferences (0.25 mM) and equimolar amounts of **NU-1000** (108.8 mg/L), phosphate and fenamiphos (0.05 mM) were shaken at 25 °C for 60 min. Afterward, the suspensions were centrifuged (9168 *g*/15 min) and the supernatants collected. Control experiments, in the absence of interferences, were also performed. The concentration of both phosphate and fenamiphos in the supernatants was analyzed as previously mentioned. All the experiments were performed in triplicate.

In order to further explore the influence of sodium hydrogen carbonate in the adsorption capacity of **NU-1000** toward phosphate and fenamiphos, additional experiments were carried out. Specifically, aqueous suspensions (1 mL) containing equimolar amounts of **NU-1000** (108.8 mg/L), phosphate and fenamiphos (0.05 mM), and different concentrations of hydrogen carbonate (0.075–2.5 mM) were shaken at 25 °C for 60 min. Afterward, the suspensions were centrifuged (9168 *g*/15 min) and the supernatants were collected and analyzed as previously described. All the experiments were performed in triplicate. $NaHCO_3$: phosphate/fenamiphos ratios ranged from 1.5:1 to 50:1.

2.2.5. Selective recovery of fenamiphos and phosphate. Recyclability of NU-1000

First, an aqueous suspension of **NU-1000** (108.8 mg/L) was stirred with an equimolar mixture of fenamiphos and phosphate (0.05 mM), (total volume of 1 mL), for 1 h at 25 °C. The suspension was centrifuged (9168 *g*/15 min) and the supernatant was collected and analyzed in order to evaluate the amount of adsorbed phosphate and fenamiphos.

Afterward, the solid was re-suspended in 1 mL of ethanol for 1 h under stirring. The ethanolic supernatant was collected by centrifugation (9168 *g*/15 min), and the concentration of fenamiphos and phosphate in this solution was spectrophotometrically quantified. Then, the resulting pellet was suspended in an aqueous solution of hydrogen carbonate (2.5 mM/1 mL) for 1 h at 25 °C (stirring). The supernatant was collected by centrifugation (9168 *g*/15 min), and the amount of phosphate was spectrophotometrically quantified. In order to regenerate NU-1000, hydrogen carbonate anions inside the cavities were chemically decomposed with a hydrochloric acid solution (2.5 mM/1 mL). After each treatment, the PXRD of the solid was collected to evaluate the structural stability of the adsorbent. For studying the recyclability of **NU-1000**, 3 successive cycles as described above were performed. In all cases, the experiments were performed in triplicate.

2.3. Studies under dynamic conditions

To evaluate the performance of **NU-1000** under dynamic conditions, an aqueous solution containing fenamiphos (0.1 mM), phosphate (0.1 mM), and $NaHCO_3$ (0.5 mM), as interferent, was pumped continuously (2 mL/min) for 120 min through a HPLC chromatographic column (length 11.5 cm, diameter 4 mm) filled with a sample of NU-1000 previously activated (25 mg, 0.012 mmol).

At different times, aliquots were collected and the concentration of fenamiphos and phosphate was spectrophotometrically quantified. Following the same procedure as in batch experiments, fenamiphos was desorbed from **NU-1000** by pumping ethanol through the column for 30 min, and the concentration of pesticide in the outer flow was quantified as previously described. Afterward, an aqueous solution of hydrogen carbonate (5 mM) was passed through the column for 1 h (2 mL/min) in order to desorb the phosphate anions that were quantified by means of the molybdenum blue method.

Finally, a solution of hydrochloric acid (5 mM) was used to regenerate the MOF for the next cycle (2 mL/min, 30 min). Three successive cycles were performed to assess the recyclability of the adsorbent under dynamic conditions.

In order to further explore the chemical stability of **NU-1000** throughout the dynamic conditions, the leaching of zirconium was analyzed by ICP-MS from different aliquots. In particular, 500 μL of the collected samples at different times, 61.5 μL of concentrated HNO_3 (69%), and 438.5 μL of water were mixed, and Zr was measured by ICP-MS analyses.

3. Results and discussion

The successful preparation of metal-organic framework **NU-1000** was first confirmed by X-ray powder diffraction (Fig. 1a) [18]. In addition, N_2 adsorption isotherm, registered after postsynthetic treatment of the material with HCl, proved its porosity. **NU-1000** showed a BET surface area of 1980 m^2/g, in agreement with the theoretical value (2280 m^2/g) [16]. As expected, the analysis of

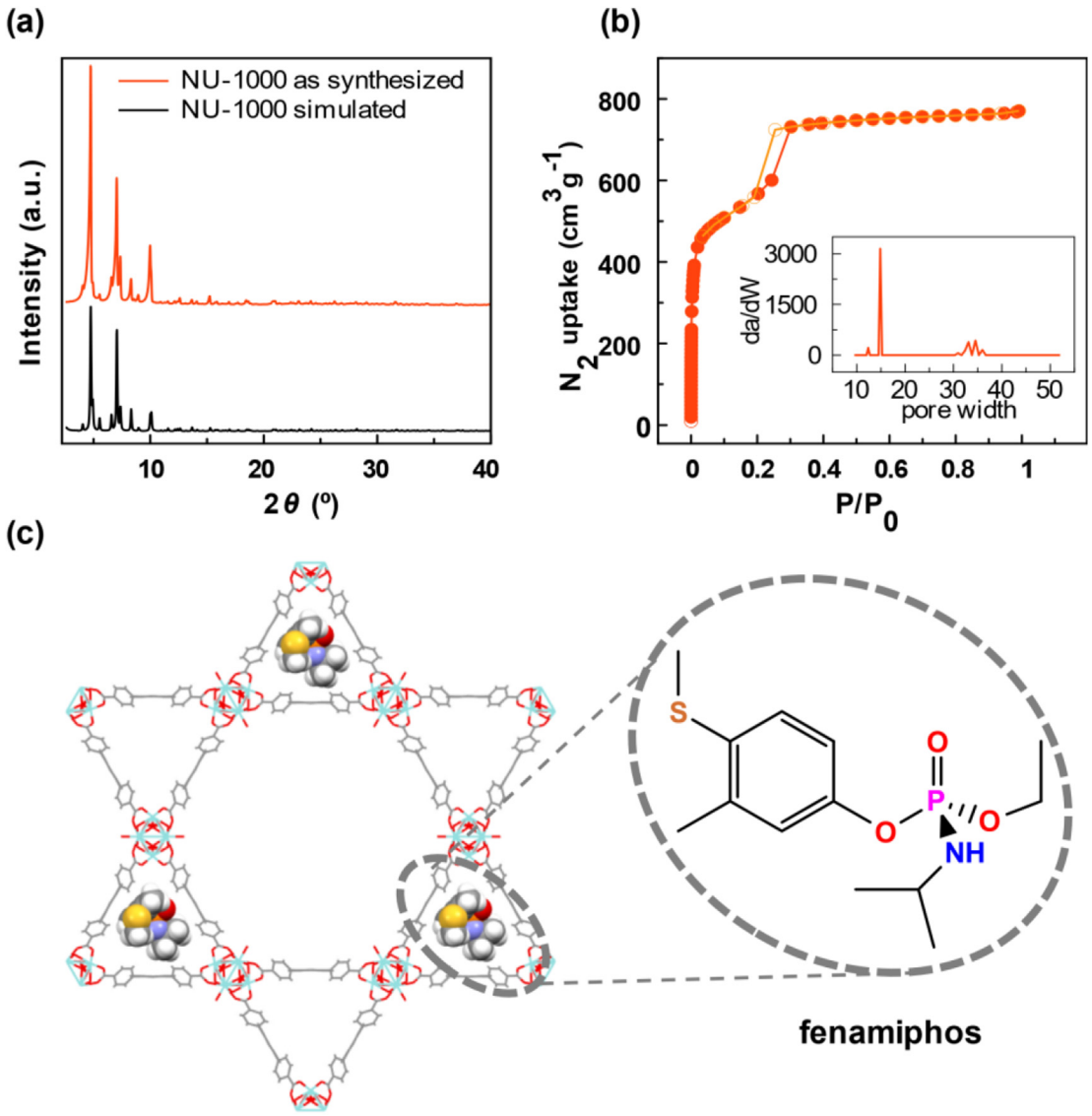

Fig. 1. Characterization of **NU-1000**: (a) XRPD patterns of simulated (black) and as-synthesized (red) material. (b) N_2 adsorption isotherm (77 K) and DFT pore size distribution. (c) Molecular modeling calculations showing the preferential accommodation of fenamiphos into the triangular micropores of **NU-1000** at lower values of loading.

pore-size distribution by DFT revealed a bimodal distribution, with pore diameters of 1.5 nm and 3.3 nm, corresponding to the triangular micropores and hexagonal mesopores of this Zr-based MOF, respectively (Fig. 1b). Additionally, Monte Carlo molecular modeling calculations [19] confirmed the accessibility of the bulky molecule fenamiphos in **NU-1000** pore structure. Consequently, the ability of the smaller phosphate ions to diffuse through the pores of **NU-1000** was assumed. The computational results indicated that the organophosphorous molecules showed preferential adsorption on the triangular micropores (Fig. 1c). The hexagonal pores accommodated additional guest molecules at higher values of loading. (Fig. S4).

Indeed, experimental data confirm the incorporation of both pollutants, from aqueous solutions, in **NU-1000** pore structure. The solid-liquid adsorption isotherms of aqueous solutions of fenamiphos and phosphate at 25 °C could be successfully fitted to a Langmuir model with maximum adsorption capacities of 1.51 mol/mol (0.7 mmol/g) and 1.46 mol/mol (0.7 mmol/g), respectively (Figs. S5 and S6). In addition, an aqueous solution of fenamiphos (0.05 mM, pH = 5.2) or phosphate (0.05 mM, pH = 6.7) was exposed to an equimolecular amount of **NU-1000** (108.8 mg/L) in order to evaluate the adsorption kinetics of these species. Both processes were fast, showing initial sharp uptakes of 93.1% ± 0.4 and 89.8% ± 6.4 after 30 min, respectively (Figs. S7 and S8). The experimental data could be fitted to a *pseudo*-second-order kinetic model (fenamiphos: $k = 0.56$ min^{-1}, $t_{1/2} = 2.1$ min; phosphate: $k = 0.06$ min^{-1}, $t_{1/2} = 16.6$ min), suggesting fast diffusion and high affinity of both phosphorous species with the pore structure. Indeed, attempts to reversibly desorb fenamiphos or phosphate from the cavities of **NU-1000**, by repetitive washing with water were unsuccessful, supporting strong interactions of both adsorbates with the MOF pore channels.

Interestingly, **NU-1000** was able to simultaneously capture fenamiphos and phosphate ions without detriment to the individual adsorption performances, showing uptakes of 97.6% ± 0.3 and 85.1% ± 4.8, respectively, after 30 min (Figs. S9 and S10). Furthermore, **NU-1000** exhibited an excellent selectivity toward the adsorption of fenamiphos in the presence of several interferences typically found in water, such as chloride, sulfate, nitrate, and hydrogen carbonate ions (interference:fenamiphos ratio

5:1) (Fig. 2a). In contrast, the presence of hydrogen carbonate significantly decreased the phosphate adsorption capacity of **NU-1000** (57.0% ± 3.5) (Fig. 2a). Additional studies revealed that hydrogen carbonate competition follows a concentration-dependent trend, leading to a 90% drop of phosphate capture for the highest assayed ratio (50:1) (Fig. 2b). Notwithstanding, the hydrogen carbonate to phosphate molar ratio used in these assays is much larger than typically found in wastewaters (1.5:1) [20]. In fact, under these more realistic conditions, **NU-1000** captures approximately 75% of phosphate in comparison to deionized aqueous solutions. Conversely, the adsorption capacity of fenamiphos by **NU-1000** remained unaltered even under the most unfavorable scenario (Fig. 2b). These results are indicative of a different mechanism for phosphate and fenamiphos adsorption into **NU-1000** pores, paving the way for the selective and independent recovery of both species.

In this sense, the extraction with ethanol (1 mL) of fenamiphos and phosphate-loaded **NU-1000** led to the complete and selective desorption of the pesticide after 1 h (Fig. S11). Interestingly, no traces of phosphate in the ethanolic solution were detected, ruling out the simultaneous release of both species. The subsequent treatment with a highly concentrated hydrogen carbonate solution (2.5 mM, 1 mL, pH = 9.8) leads to the recovery of a significant amount of phosphate (74.3 ± 3.0%) after 1 h (Fig. S11).

Once both pollutants were recovered, we proceeded to regenerate the **NU-1000** adsorbent. With this aim, the resulting material was treated with diluted hydrochloric acid (2.5 mM) to decompose the entrapped hydrogen carbonate anions. To prove the impact of the adsorption, desorption, and regeneration treatments on the structural integrity of the adsorbent, both **NU-1000** solid and eluted solutions were analyzed by XRPD and UV-spectroscopy, respectively. Although an important loss of crystallinity was observed (Fig. S12), no leaching of the organic ligand TBAPy was detected (Fig. S13), confirming the chemical stability of the MOF under the assayed conditions.

The recyclability of the adsorbent was evaluated over two additional cycles. The results revealed that **NU-1000** maintained reasonable reusability toward the adsorption of fenamiphos and phosphate with drops of 20% and 35% between the first and third cycles, respectively (Fig. S14). Likewise, the selective recovery of fenamiphos and phosphate followed a similar trend, with respective desorption rates of 81% and 63% for the third cycle.

To date, most of the studies on MOFs for capturing pollutants in aqueous solutions are limited to batch experiments in static conditions [9–15]. Although these studies allow the comparison of the behavior of different adsorbents, they are far from real practical applications. In order to get a more realistic insight into the performance of **NU-1000** toward the adsorption-desorption of fenamiphos and phosphate, different experiments, under dynamic conditions on an **NU-1000** HPLC packed column, were carried out. Noteworthy, the concentration of phosphate (0.1 mM) employed was in the range of those found in eutrophicated waters [21] or wastewaters [20].

In a typical experiment to evaluate the decontamination capacity of this adsorbent, an aqueous solution containing an equimolar mixture of phosphate and fenamiphos as pollutants (0.1 mM) and hydrogen carbonate as interference (0.5 mM) was continuously flowed (2 mL/min) through a HPLC-column packed with **NU-1000** (25 mg) (Fig. 3a). First, a good adsorption performance for both phosphate and fenamiphos was observed. Indeed, in the first cycle, fenamiphos followed a steady rhythm of adsorption with a maximum cumulative uptake of 0.89 mol/mol after 120 min (Fig. 3b). On the other hand, phosphate was quickly captured, reaching saturation after 20 min (cumulative adsorption of 0.19 mol/mol) (Fig. 3c). As expected, the adsorption capacity of **NU-1000** toward fenamiphos was superior to the one quantified for phosphate, probably due to the competitive adsorption of the large excess of hydrogen carbonate (5 folds).

Regarding the desorption process, the pollutants were spectrophotometrically monitored in the eluted flow following a similar strategy than in the batch studies. The pesticide was first recovered from the column using EtOH as eluent (2 mL/min) while phosphate ions were released using the above-mentioned hydrogen carbonate ion-exchange strategy (5 mM, 2 mL/min). The treatment with ethanol allowed fast desorption of fenamiphos (*c.a.* 10 min), while the exchange of phosphate with hydrogen carbonate was completed in approximately 35 min, bringing to light the strong affinity of Zr centers of **NU-1000** for phosphate anions (Fig. 3b and c) [22]. Afterward, the adsorbent was regenerated by flowing a diluted hydrochloric acid solution (5 mM, 2 mL/min) for 30 min.

Finally, in order to evaluate the recyclability of **NU-1000** adsorbent, two subsequent dynamic adsorption-desorption cycles were registered. The results show that the kinetic profiles of both adsorption and desorption processes are maintained over the

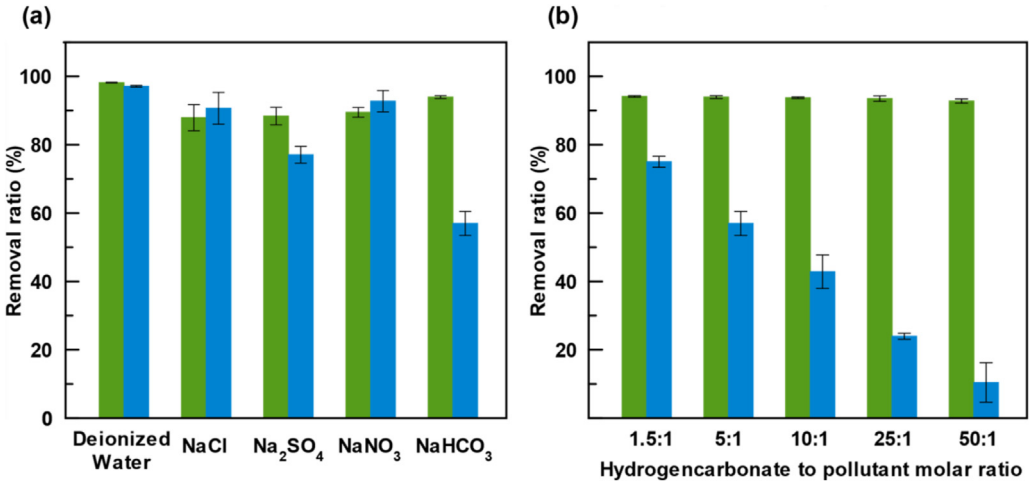

Fig. 2. (a) Pollutant adsorption by **NU-1000** in the presence of different interferences (interference to pollutant molar ratio 5:1) (b) Impact of increasing concentrations of hydrogen carbonate on the pollutant adsorption by **NU-1000** (hydrogen carbonate to pollutant molar ratio from 1.5:1 to 50:1). Removal ratio of fenamiphos (green bars) and phosphate (blue bars).

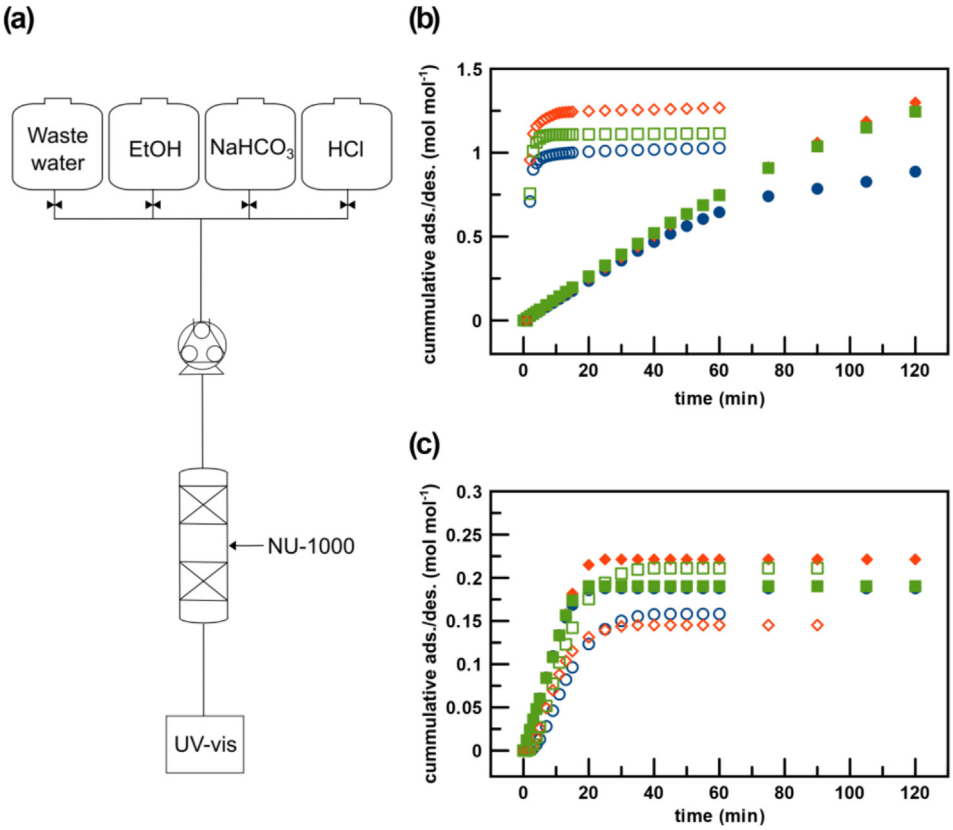

Fig. 3. Adsorption and selective recovery of fenamiphos and phosphate from wastewater under dynamic conditions. (a) Schematic representation of the experimental setup of **NU-1000** loaded HPLC column for the dynamic studies. (b) Cumulative adsorption (filled markers) and desorption (empty markers) of fenamiphos. Ethanol was used as eluent during the desorption process (c) Cumulative adsorption (filled markers) and desorption (empty markers) of phosphate. The desorption of phosphate was performed by-exchange with hydrogen carbonate solution (5 mM). Experimental details: Stainless steel column of 4 mm inner diameter filled with 25 mg of **NU-1000**. Simulated wastewater to be purified: 0.1 mM of phosphate, 0.1 mM of fenamiphos and 0.5 mM of hydrogen carbonate. Solution for regenerating the adsorbent between cycles: 5 mM of hydrochloric acid. All experiments were performed at 25 °C and flow rate = 2 mL/min 1st cycle (blue circles), 2nd cycle (red triangles), and 3rd cycle (green squares).

essayed three consecutive cycles (Fig. 3). Noteworthy, the recovery ratios were close to 100%, which may be explained taking into account that, under these dynamic conditions, fresh desorbing agent (i.e. ethanol or hydrogen carbonate) is continuously in contact with the adsorbent forcing the desorption of the adsorbate molecules from the pores. Additionally, ICP-MS analysis over three cycles demonstrated that no Zr leaching occurred, proving the chemical stability of **NU-1000** under these experimental conditions close to real water treatments.

4. Conclusions

In conclusion, we have demonstrated the good performance of **NU-1000** as a dual adsorbent of two different P-based water pollutants, namely fenamiphos and phosphate, under dynamic conditions and in the presence of relevant interferences, typically found in eutrophicated and wastewater. Moreover, taking advantage of the different adsorption mechanisms for these two species, namely phosphate coordination to the Zr_6 metal cluster and fenamiphos van der Waals interactions with the pore walls, we have developed a three-step strategy to selectively recover them and subsequently regenerate the adsorbent. The adsorbent has proved to exhibit good reusability, allowing the performance of three adsorption-desorption cycles with recovery ratios close to 100%. These results represent a step forward toward the application of MOF materials for wastewater treatment since previously reported studies are limited to the detoxification of a single phosphorous pollutant under static batch conditions. Likewise, the phosphate selectively recovered could be reused as a phosphorous fertilizer, contributing to the P circular economy. On the basis of these results, we envision that Zr-based MOFs will play an important role in phosphorous sustainability.

Author contributions

Lydia González: Investigation, Visualization. **Francisco J. Carmona:** Conceptualization, Methodology, Investigation, Writing - Original Draft, Reviewing and Editing, Funding acquisition. **Natalia M. Padial:** Investigation. **Jorge A. R. Navarro:** Formal Analysis, Supervision, Writing - Reviewing and Editing, Funding acquisition. **Elisa Barea:** Writing - Original Draft, Reviewing and Editing, Project administration, Funding acquisition. **Carmen R. Maldonado:** Writing - Original Draft, Reviewing and Editing, Project administration, Funding acquisition.

Data availability

The data used to support the findings of this study are included in the article.

Declaration of competing interest

The authors declare that they have no known competing financial interests or personal relationships that could have appeared to influence the work reported in this paper.

Acknowledgments

The authors express their thanks for the financial support provided by the Marie Skłodowska-Curie Individual Fellowships (H2020-MSCA-IF-2019-EF-ST-888972-PSustMOF, F.J.C.; H2020-MSCA-IF-2016-GF-749359-EnanSET, N.M.P.) within the European Union H2020 programme and EU FEDER. MINECO (CTQ2017-84692-R, PID2020-113608RB-I00, PEJ2018-004022-A), Universidad de Granada (Plan Propio de Investigación and Programa Operativo FEDER Andalucía 2014-2020: B-FQM-364-UGR18), Junta de Andalucía (P18-RT-612) and 2020 Post-doctoral Junior Leader−Retaining Fellowship, la Caixa Foundation (ID 100010434 and fellowship code LCF/BQ/PR20/11770014, N.M.P.) are also acknowledged for funding. Funding for open access charge: Universidad de Granada / CBUA.

Appendix A. Supplementary data

Supplementary data to this article can be found online at https://doi.org/10.1016/j.mtchem.2021.100596.

References

[1] FAO, World Food Situation, 2020. Http://Www.Fao.Org/Worldfoodsituation/Csdb/En/. (Accessed 26 June 2021). http://www.fao.org/worldfoodsituation/csdb/en/.
[2] H. Soreq, S. Seidman, Acetylcholinesterase — new roles for an old actor, Nat. Rev. Neurosci. 2 (2001) 294−302, https://doi.org/10.1038/35067589.
[3] M. Wang, C. Hu, B.B. Barnes, G. Mitchum, B. Lapointe, J.P. Montoya, The great Atlantic Sargassum belt, Science 364 (2019) 83−87, https://doi.org/10.1126/science.aaw7912.
[4] M. Mon, R. Bruno, J. Ferrando-Soria, D. Armentano, E. Pardo, Metal-organic framework technologies for water remediation: towards a sustainable ecosystem, J. Mater. Chem. A. 6 (2018) 4912−4947, https://doi.org/10.1039/c8ta00264a.
[5] S. Rojas, P. Horcajada, Metal-organic frameworks for the removal of emerging organic contaminants in water, Chem. Rev. 120 (2020) 8378−8415, https://doi.org/10.1021/acs.chemrev.9b00797.
[6] G.I. Tovar Jimenez, A. Valverde, C. Mendes-Felipe, S. Wuttke, A. Fidalgo-Marijuan, E.S. Larrea, L. Lezama, F. Zheng, J. Reguera, S. Lanceros-Méndez, M.I. Arriortua, G. Copello, R.F. Luis, Chitin/metal-organic framework composites as wide-range adsorbent, ChemSusChem 14 (2021) 1−11, https://doi.org/10.1002/cssc.202100675.
[7] C.O. Audu, H.G.T. Nguyen, C.Y. Chang, M.J. Katz, L. Mao, O.K. Farha, J.T. Hupp, S.T. Nguyen, The dual capture of AsV and AsIII by UiO-66 and analogues, Chem. Sci. 7 (2016) 6492−6498, https://doi.org/10.1039/c6sc00490c.
[8] J.H. Cavka, S. Jakobsen, U. Olsbye, N. Guillou, C. Lamberti, S. Bordiga, K.P. Lillerud, A new zirconium inorganic building brick forming metal organic frameworks with exceptional stability, J. Am. Chem. Soc. 130 (2008) 13850−13851, https://doi.org/10.1021/ja8057953.
[9] M. Liu, S. Li, N. Tang, Y. Wang, X. Yang, S. Wang, Highly efficient capture of phosphate from water via cerium-doped metal-organic frameworks, J. Clean. Prod. 265 (2020) 121782, https://doi.org/10.1016/j.jclepro.2020.121782.
[10] X. Min, X. Wu, P. Shao, Z. Ren, L. Ding, X. Luo, Ultra-high capacity of lanthanum-doped UiO-66 for phosphate capture: unusual doping of lanthanum by the reduction of coordination number, Chem. Eng. J. 358 (2019) 321−330, https://doi.org/10.1016/j.cej.2018.10.043.
[11] Y. Gu, D. Xie, Y. Ma, W. Qin, H. Zhang, G. Wang, Y. Zhang, H. Zhao, Size modulation of zirconium-based metal organic frameworks for highly efficient phosphate remediation, ACS Appl. Mater. Interfaces 9 (2017) 32151−32160, https://doi.org/10.1021/acsami.7b10024.
[12] R.J. Drout, L. Robison, Z. Chen, T. Islamoglu, O.K. Farha, Zirconium metal−organic frameworks for organic pollutant adsorption, Trends Chem 1 (2019) 304−317, https://doi.org/10.1016/j.trechm.2019.03.010.
[13] Q. Yang, J. Wang, X. Chen, W. Yang, H. Pei, N. Hu, Z. Li, Y. Suo, T. Li, J. Wang, The simultaneous detection and removal of organophosphorus pesticides by a novel Zr-MOF based smart adsorbent, J. Mater. Chem. A. 6 (2018) 2184−2192, https://doi.org/10.1039/c7ta08399h.
[14] A. Pankajakshan, M. Sinha, A.A. Ojha, S. Mandal, Water-stable nanoscale zirconium-based metal-organic frameworks for the effective removal of glyphosate from aqueous media, ACS Omega 3 (2018) 7832−7839, https://doi.org/10.1021/acsomega.8b00921.
[15] X. Zhu, B. Li, J. Yang, Y. Li, W. Zhao, J. Shi, J. Gu, Effective adsorption and enhanced removal of organophosphorus pesticides from aqueous solution by Zr-Based MOFs of UiO-67, ACS Appl. Mater. Interfaces 7 (2015) 223−231, https://doi.org/10.1021/am5059074.
[16] T.C. Wang, N.A. Vermeulen, I.S. Kim, A.B.F. Martinson, J. Fraser Stoddart, J.T. Hupp, O.K. Farha, Scalable synthesis and post-modification of a mesoporous metal-organic framework called NU-1000, Nat. Protoc. 11 (2016) 149−162, https://doi.org/10.1038/nprot.2016.001.
[17] L. Drummond, W. Maher, Chimica Acta (1995) 2670.
[18] J.E. Mondloch, W. Bury, D. Fairen-Jimenez, S. Kwon, E.J. Demarco, M.H. Weston, A.A. Sarjeant, S.T. Nguyen, P.C. Stair, R.Q. Snurr, O.K. Farha, J.T. Hupp, Vapor-phase metalation by atomic layer deposition in a metal-organic framework, J. Am. Chem. Soc. 135 (2013) 10294−10297, https://doi.org/10.1021/ja4050828.
[19] BIOVIA, Materials Studio, 2018.
[20] M.B. Pescod, Wastewater Treatment and Use in Agriculture - FAO Irrigation and Drainage, 1992.
[21] C.E. Boyd, Phosphorous, in: Water Qual., Springer International Publishing, 2015, pp. 243−261.
[22] Y. Su, H. Cui, Q. Li, S. Gao, J.K. Shang, Strong adsorption of phosphate by amorphous zirconium oxide nanoparticles, Water Res. 47 (2013) 5018−5026, https://doi.org/10.1016/j.watres.2013.05.044.